AJNR Am J Neuroradiol 23:1747–1756, November/December 2002

The Substantia Nigra in Parkinson Disease: Proton Density–Weighted Spin-Echo and Fast Short Inversion Time Inversion-Recovery MR Findings

Hirobumi Oikawa, Makoto Sasaki, Yoshiharu Tamakawa, Shigeru Ehara, and Koujiro Tohyama

BACKGROUND AND PURPOSE: **A reduction in the area of the substantia nigra (SN) has been shown in patients with Parkinson disease. The substantia nigra is anteroinferolateral to the red nucleus, and it is important to precisely locate its true anatomic location to accurately measure SN area. Our purpose was to determine the exact location of the substantia nigra by correlating imaging and anatomic findings. We also attempted to quantitate SN area in patients with Parkinson disease compared with that in healthy control subjects on the basis of proton density–weighted spin-echo (SE) and fast short inversion time inversion-recovery (STIR) MR imaging findings.**

METHODS: **In four healthy volunteers, dual-echo SE and fast STIR MR images were obtained in three orthogonal planes and an oblique coronal plane. These images were correlated with anatomic specimens to determine the location of the SN. The area of the SN was also measured on oblique coronal fast STIR images obtained at a plane perpendicular to the SN in 22 patients with Parkinson disease and in 22 age- and sex-matched healthy volunteers.**

RESULTS: **The true anatomic location of the SN, anteroinferolateral to the red nucleus, was accurately identified, not on T2-weighted images, but on proton density–weighted SE images and fast STIR images as an area of hyperintense gray matter. The hypointense area seen on T2-weighted images corresponded to the anterosuperior aspect of the SN and to the adjacent crus cerebri. No statistically significant differences were noted in the size of the SN when the oblique coronal images of patients with Parkinson disease were compared with those of the control groups.**

CONCLUSION: **The SN is located mainly beneath the red nucleus. Its location cannot be determined on the basis of T2-weighted imaging results but rather on the basis of proton density–weighted SE or fast STIR findings. SN volume loss is not found in Parkinson disease, and this finding is compatible with that of recent pathology reports in the literature.**

The signal intensity of iron-containing deep nuclei, such as the globus pallidus and red nucleus, is decreased on T2-weighted MR images (1, 2). The substantia nigra (SN), which also contains iron, can be distinguished as a two-layered structure on axial T2-weighted images at the level of the upper midbrain. A hypointense area in the posterior region of the crus cerebri is considered to be the pars reticulata (SNr), and a relatively hyperintense area between the SNr and red nucleus is the pars compacta (SNc). This knowledge has been applied in the evaluation of patients with Parkinson disease, and narrowing of the SNc area or restoration of the SNr signal intensity is present in patients with Parkinson disease (2–4). However, several neuroimaging articles have described that the SN is visible on proton density–weighted or short inversion time inversion-recovery (STIR) images, although the SNr and SNc cannot be distinguished (5–9). In these articles and in neuroanatomic atlases, the described location of the SN, which is anteroinferolateral to the red nucleus (Fig 1), does not match that of the two-layered structure depicted

Received March 21, 2001; accepted after revision July 31, 2002.

From the Department of Radiology (H.O., M.S., Y.T., S.E.), High Field Magnetic Resonance Imaging Research Institute (M.S.), and the Department of Neuroanatomy (K.T.), Iwate Medical University, Uchimaru, Morioka, Japan.

Supported in part by Grants-in-Aid for Advanced Medical Science Research from the Ministry of Science, Education, Sports and Culture, Japan.

Address reprint requests to Hirobumi Oikawa, MD, Department of Radiology, Iwate Medical University School of Medicine, 19–1 Uchimaru, Morioka 020-8505, Japan.

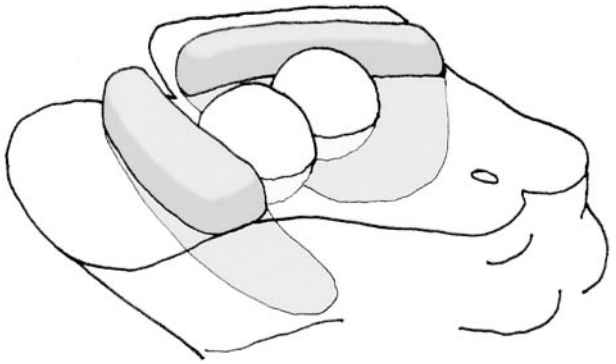

FIG 1. Schematic drawing of the three-dimensional anatomy of the SN from the left superoposterolateral aspect. The SN is located mainly beneath the red nucleus.

on T2-weighted images (10–12). The purpose of this study was to investigate the MR characteristics of the SN area in healthy subjects compared with those in patients with Parkinson disease on the basis of proton density–weighted and fast STIR imaging findings.

Methods

Subjects

Initial MR imaging studies of the SN were prospectively performed in healthy volunteers and in consecutive patients with a clinically established diagnosis of Parkinson disease between August 1999 and September 2000.

To explore the MR imaging anatomy of the SN, four volunteers (one male and three female; age range, 54–60 years; mean age ± SD, 57.3 years ± 2.2) were examined. Twenty-two patients with Parkinson disease (nine male and 13 female; age range, 43–72 years; mean age ± SD, 59.8 years ± 9.2) and 22 healthy volunteers (10 male and 12 female; age range, 43–74 years; mean age ± SD, 58 years ± 8.8) underwent MR imaging. Patients were evaluated for the severity of the disease by using the Hoehn-Yahr scale. Eleven patients were classified as having mild disease (stage 1 or 2), and 11 had moderate disease (stage 3). The duration of the disease was 0.5–11.9 years (mean ± SD, 2.7 years ± 2.6). All subjects provided written informed consent before participating in this study.

MR Imaging

A 1.5-T superconductive system (Signa Lx; GE Medical Systems, Milwaukee, WI) was used for MR imaging. The fol-

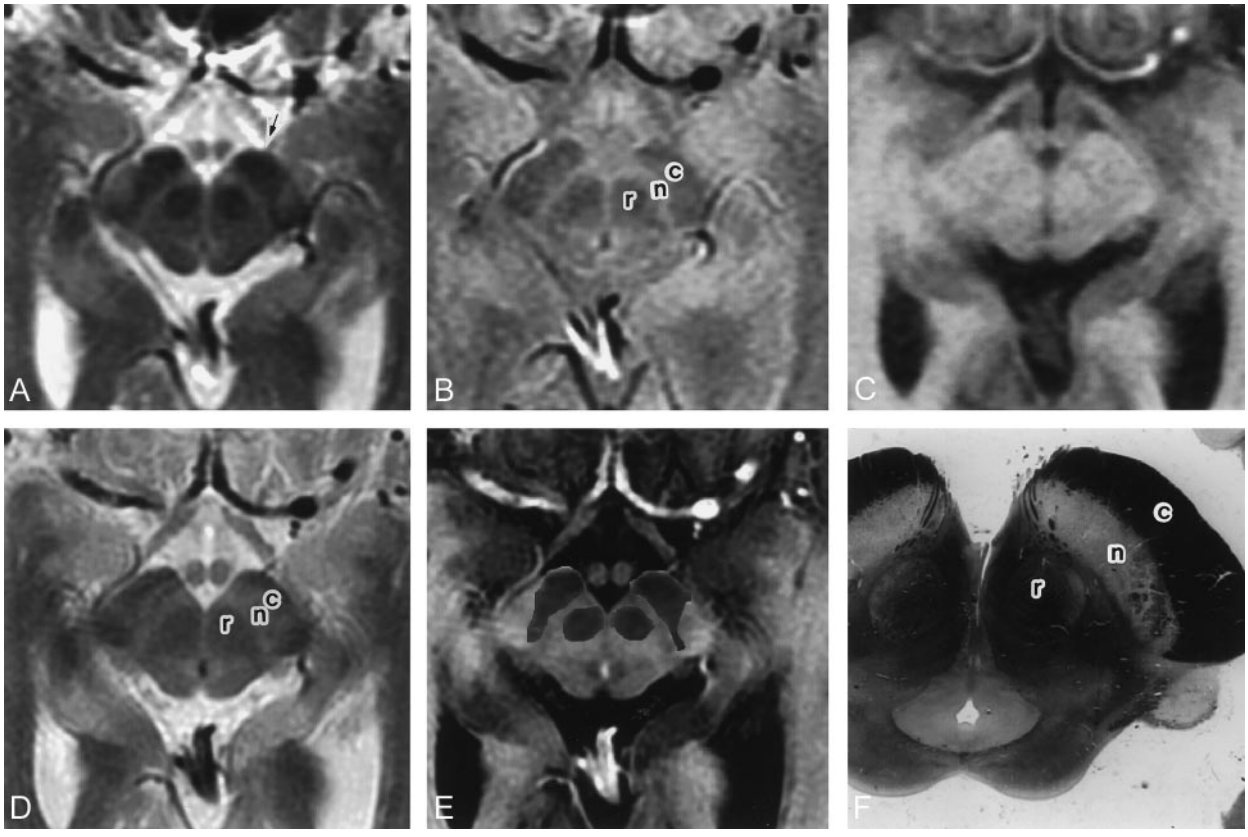

FIG 2. Axial MR images through the upper midbrain.

A, Axial T2-weighted image in a healthy control subject, a 55-year-old woman. A hypointense area, believed to be SNr, is located in the anteromedial part of the crus cerebri (*arrow*). No hyperintense gray matter area, representing the SN, is visible.

B, Proton density–weighted image in the same section as in *A*. The SN (*n*) is clearly identified as an area of hyperintense gray matter surrounded by the hypointense red nucleus (*r*) and the crural fibers (*c*).

C, T1-weighted image in the same section as in *A*. The SN is not evident.

D, Fast STIR image in the same section as in *A*. The SN (*n*) is readily identified as a structure with gray matter signal intensity. The red nucleus (*r*) with surrounding white matter and the crural fibers (*c*) are identified as areas with relatively low signal intensity.

E, Video-reversed fast STIR image onto which the hypointense areas on a T2-weighted image are superimposed (*shaded areas*). The hypointense area on the T2-weighted image includes the crural fibers and the anterior part of the SN.

F, Corresponding axial-section specimen obtained from a human cadaver.

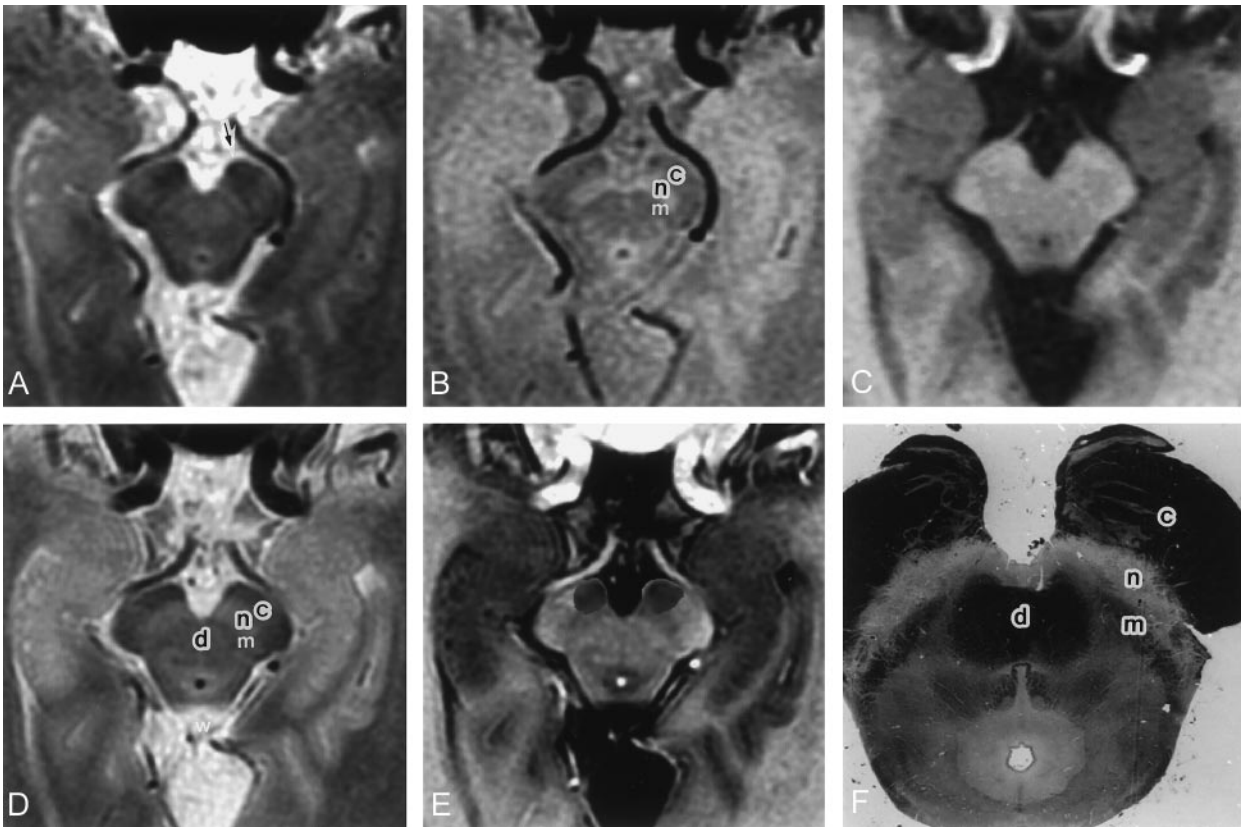

FIG 3. Axial MR images through the lower midbrain.

A, Axial T2-weighted image in the same control subject as in Figure 2. A hypointense area is visible on only the anteromedial end of the crus cerebri (*arrow*). An area with relatively high signal intensity suggestive of the SN is not depicted.

B, Proton density–weighted image in the same section as in *A*. The SN (*n*) is clearly depicted as a structure with hyperintense gray matter between the crural fibers (*c*) and the medial lemniscus (*m*).

C, T1-weighted image obtained at the same section as in *A*. The SN is not visible.

D, Fast STIR image in the same section as in *A*. The SN (*n*) is identified as an area of hyperintense gray matter posterior to the crural fibers (*c*). The medial lemniscus (*m*) and the decussation of superior cerebellar peduncle (*d*) show relatively low signal intensity.

E, Video-reversed fast STIR image onto which the hypointense areas on a T2-weighted image are superimposed (*shaded areas*). The hypointense areas on the T2-weighted image are located on the anteromedial part of the peduncular fibers, but they barely include the SN.

F, Axial-section specimen obtained in a human cadaver through the lower end of the midbrain. The SN (*n*) is not present on this section. It is located between the crural fibers cerebri (*c*) and medial lemniscus (*m*).

lowing pulse sequences were used: conventional dual-echo spin-echo (SE) sequence (TR/TE/NEX, 2500/34 and 100/1), fast STIR sequence (TR/TI/TE_{eff}/NEX, 4000/120/363; echo train length, 12, echo spacing, 12 ms; tailored radio frequencies). We used a relatively short inversion time to improve the signal-to-noise ratio and to enhance gray matter–white matter contrast.

SE imaging and fast STIR imaging were performed with 4-mm-thick sections, a 1.5-mm intersection gap, and a 22-cm field of view (FOV) in three orthogonal and oblique coronal directions. The matrix size was 256 × 192 on the SE images and 256 × 256 on the fast STIR images. Axial images were oriented parallel to the anterior commissure–posterior commissure (AC-PC) line, and they were carefully positioned to include sections through the upper midbrain (red nucleus and superior colliculus) and the lower midbrain (decussation of superior cerebellar peduncle and inferior colliculus). Coronal images were oriented perpendicular to the AC-PC line. Sagittal images were also obtained. Oblique coronal images were set at 45° to the AC-PC line, because this orientation is almost perpendicular to the SN, according to the atlas of Talairach (13). The sections were carefully positioned to include the planes through the posterior commissure and the superior colliculus, which were used to measure the area of the SN. These oblique coronal images enabled us to avoid partial-volume effects and to measure of the SN.

We also obtained 3D T1-weighted images with a 3D Fourier transform fast spoiled gradient-recalled acquisition in the steady state (FSPGR) sequence, (TR/TE, 11.7/2.4; flip angle, 20°). FSPGR sections were 1.3 mm thick, with a 22-cm FOV and a 256 × 224 × 128 matrix size. Images obtained in four directions corresponding with the SE and fast STIR images were reconstructed from the 3D datasets.

Anatomic Analysis

To clarify the location of the SN on the MR images, we compared the anatomic appearances of the cadaveric specimens with the MR images obtained in four directions. After 10% formaldehyde fixation and paraffin embedding, axial sections through the upper and lower midbrain and oblique coronal sections through the red nucleus of human brains were obtained from three cadavers (59-year-old man, 52-year-old man) without Parkinson disease or other CNS diseases. The section thickness was 26 μm, and a combination of the Weigert myelin stain and the Nissl stain was used. One of the authors (K.T.) prepared the specimens. We also used coronal and sagittal gross specimens through the red nucleus from two

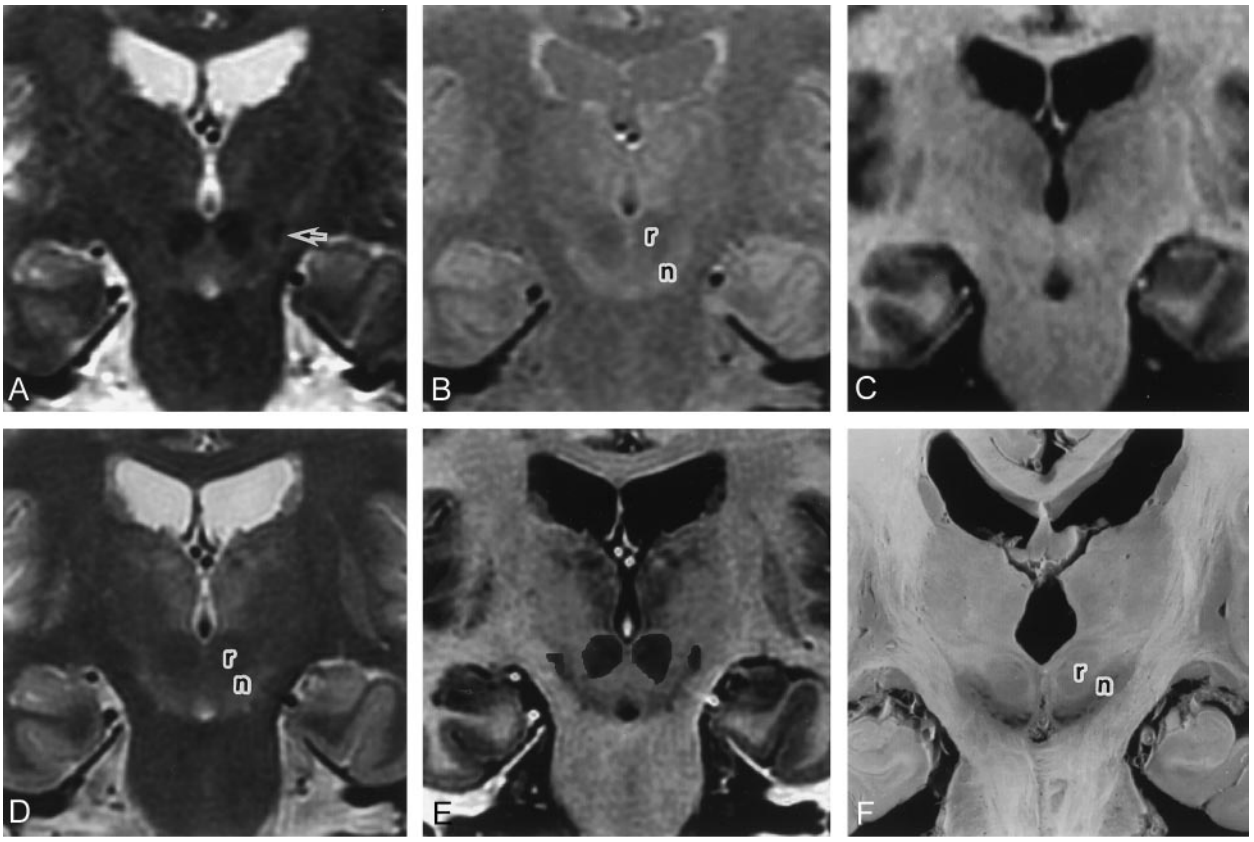

FIG 4. Coronal MR images through the red nucleus.

A, T2-weighted image from a control subject, a 58-year-old woman. The red nucleus is depicted as a round hypointense structure. Another hypointense area is lateral to the red nucleus (*arrow*).

B, Proton density–weighted image in the same section as in *A*. The SN (*n*) is depicted as an area of hyperintense gray matter inferolateral to the red nucleus (*r*).

C, T1-weighted image obtained in the same section as in *A*. The SN is not visible.

D, Coronal fast STIR image obtained in the same section as in *A*. The SN (*n*) is readily identified as an area of hyperintense gray matter. The red nucleus (*r*) is also depicted.

E, Video-reversed fast STIR image onto which the hypointense regions on a T2-weighted image are superimposed (*shaded areas*). The hypointense areas on the T2-weighted image are located on only the superolateral end of the SN.

F, Gross specimen of the human brain. The SN (*n*) is identified as a tilted bandlike area inferolateral to the red nucleus (*r*). The SN is present through the entire length of the midbrain, and its lower half is located beneath the red nucleus.

cadavers (71 year-old man, 61-year-old woman) without Parkinson disease or other CNS diseases. Two radiologists (H.O., M.S.) reviewed the anatomic specimens and the MR images to estimate the location of the SN on the MR images.

Analysis in Parkinson Disease

One of the authors (H.O.) measured the area of the SN in a blinded fashion. The measurements were performed on the oblique coronal fast STIR images perpendicular to the SN and on the axial T2-weighted images through the upper midbrain. A workstation (Advantage Windows; GE Medical Systems) was used. After carefully setting the window level, window width, and magnification, regions of interest were manually traced with a mouse-driven cursor on a monitor. On the oblique coronal fast STIR images, we measured the area of the SN and the midbrain on two contiguous sections through the posterior commissure and the superior colliculus. We also measured the thickness of the SN on the oblique coronal fast STIR images through the posterior commissure. We normalized the area of the SN by using the area of the midbrain to adjust for age-related changes (14). On the axial T2-weighted images, we measured the width of the relatively hyperintense band between two hypointense areas, as described in previous reports (3). The measurements were performed at the same levels in all of the patients.

Statistical comparisons were based on results of the Student and Welch *t* tests. *P* values less than .05 were considered to indicate a significant difference.

Results

Normal MR Findings

On the proton density–weighted and fast STIR images, an area of gray matter signal intensity that suggested the SN was depicted in the axial planes at the level of the upper and lower midbrain (Figs 2 and 3). On the coronal and sagittal images through the red nucleus, a tilted band with gray matter signal intensity was found inferolateral and anteroinferior to the red nucleus, respectively (Figs 4 and 5). These findings corresponded well to those of the specimens and were not visible on the T2-weighted images (Figs 2–5).

On T2-weighted images, the area of low signal intensity corresponding to the SNr and the area of relatively high signal intensity corresponding to the SNc were depicted, as reported in previous articles

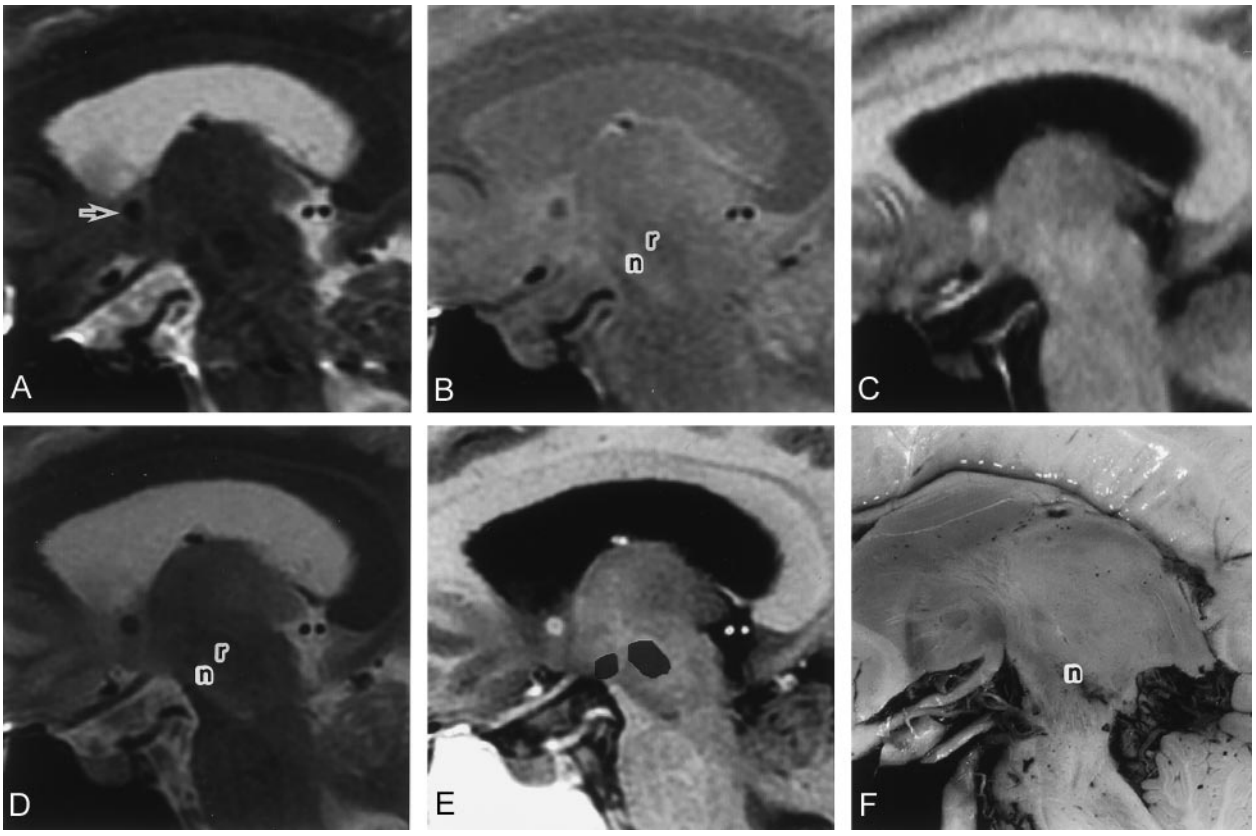

FIG 5. Sagittal MR images through the red nucleus.

A, Sagittal T2-weighted image obtained in a control subject, a 55-year-old woman. Hypointense areas are visible at the red nucleus and at the anterior margin of the midbrain (*arrow*). The boundary of the hyperintense band is unclear at the level of lower midbrain.

B, Proton density–weighted image in the same section as in *A*. The SN is identified as a tilted gray matter structure (*n*) anteroinferior to the red nucleus (*r*).

C, T1-weighted image in the same section as in *A*. The SN is not identified.

D, Fast STIR image at the same section. The SN is identified as a bandlike structure with gray matter signal intensity (n) that is mainly located anteroinferior to the red nucleus (*r*).

E, Video-reversed fast STIR image onto which the hypointense regions of a T2-weighted image are superimposed (*shaded areas*). The low-signal-intensity area on the T2-weighted image includes the crural fibers and only the anterosuperior end of the SN.

F, Sagittal gross specimen of the human brain slightly lateral to the MR images. The SN (*n*) is identified as a tilted band-shaped area.

(1–4). The locations of the hypointense areas were minimally correlated to those on the specimens and those on proton density–weighted and STIR images. On axial images, the hypointense area extended anterior to the anteromedial end of the crus cerebri; this finding suggested that the area included medial parts of the crural fibers (Figs 2 and 3). Moreover, the hypointense area seemed not to exclude the area of gray matter seen on the proton density–weighted or STIR images at the lower midbrain. Coronal and sagittal images showed low signal intensity at only the upper end of gray matter (Figs 4 and 5).

On the oblique coronal proton density–weighted and fast STIR images perpendicular to the SN, the SN was depicted as a well-marginated area of gray matter signal intensity (Fig 6); the SN was not evident on the T2-weighted images (Fig 6). These findings suggested that the SN did not show low signal intensity except at its superoanteromedial part (Fig 7, Table 1).

Measurement of the Substantia Nigra

To avoid intrarater variability, every measurement was performed three times, and the measurements were averaged. The intraclass correlation coefficients (*Ri*) for these measurements were 0.87–0.99 for areas of the SN and midbrain and 0.68–0.90 for the width of the hyperintense band on T2-weighted images.

The area of the SN was 42.4–59.2 mm^2 in patients with Parkinson disease (mean ± SD, 51.2 mm^2 ± 5.1), and it was 44.3–63.2 mm^2 (mean ± SD, 53.1 mm^2 ± 6.2) in the control group ($P > .05$). The area of the SN normalized with that of the midbrain was 9.3 mm^2 in Parkinson disease and 9.1 mm^2 in the control group ($P > .05$). The thickness of the SN was from 3.6–4.8 mm in the patients (mean ± SD, 4.3 mm ± 0.4) and 3.5–5.1 mm (mean ± SD, 4.4 mm ± 0.4) in the control group ($P > .05$). Atrophy of the midbrain was not identified in patients with Parkinson disease. On the other hand, the width of the hyperintense band on the T2-weighted images was 1.3–2.3 mm (mean ± SD, 1.6 mm ± 0.2) in the Parkinson disease group and 1.3–2.3 mm (mean ± SD, 1.7 mm ± 0.3) in the control group ($P > .05$). The results did not reveal a statistically significant difference between the patients with Parkinson disease and the control group in any parameter (Figs 8 and 9;

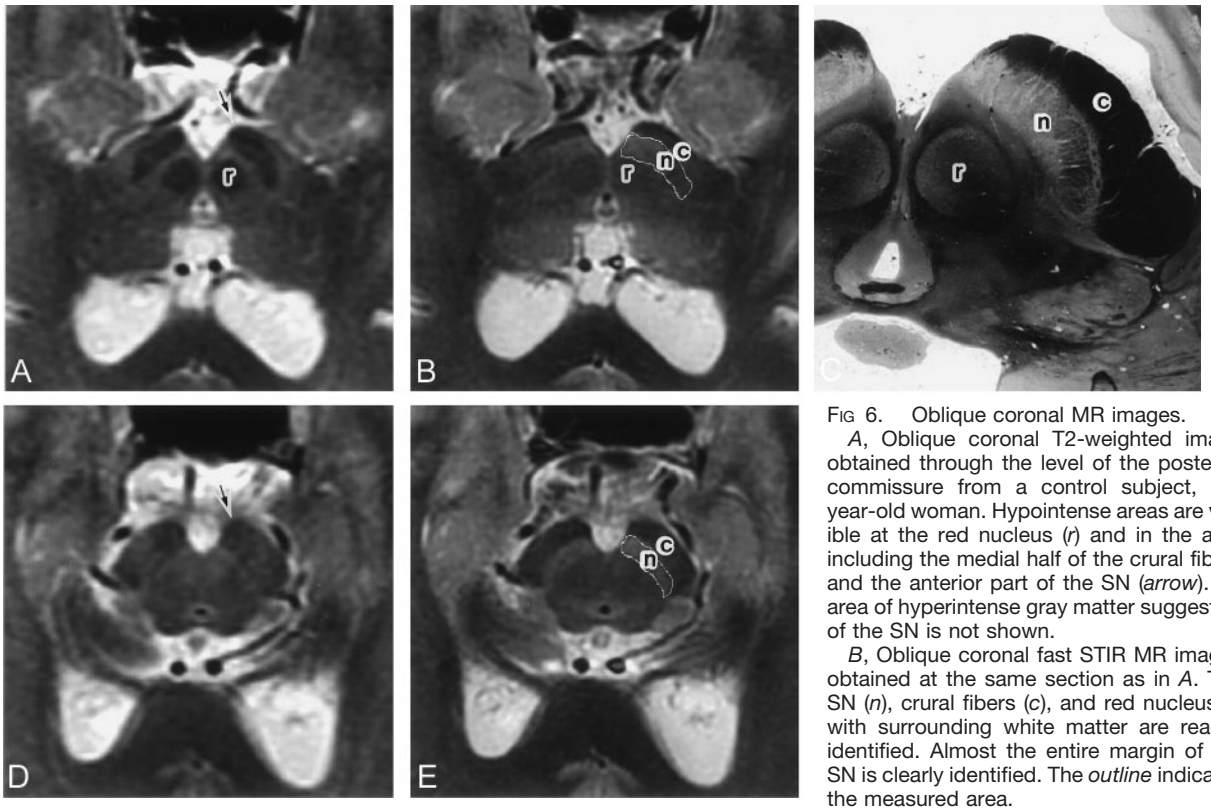

FIG 6. Oblique coronal MR images.

A, Oblique coronal T2-weighted image obtained through the level of the posterior commissure from a control subject, 58-year-old woman. Hypointense areas are visible at the red nucleus (*r*) and in the area including the medial half of the crural fibers and the anterior part of the SN (*arrow*). An area of hyperintense gray matter suggestive of the SN is not shown.

B, Oblique coronal fast STIR MR images obtained at the same section as in *A*. The SN (*n*), crural fibers (*c*), and red nucleus (*r*) with surrounding white matter are readily identified. Almost the entire margin of the SN is clearly identified. The *outline* indicates the measured area.

C, Corresponding oblique coronal section of the human specimen. The SN (*n*) is identified as a crescent gray matter structure located posterior to the crural fibers (*c*) and anterolateral to the red nucleus (*r*).

D, Oblique coronal T2-weighted image through the level of the superior colliculus obtained in the same subject as in *A*. The hypointense area is depicted at only the anteromedial aspect of the crus cerebri (*arrow*). A hyperintense area suggestive of the SN is not identified.

E, Oblique coronal fast STIR image obtained at the same section as in *D*. A bandlike structure with hyperintense gray matter that represents the SN (*n*) is depicted posteromedial to the hypointense crural fibers (*c*). The *outline* indicates the measured area.

Table 2). No signal intensity changes were noted in the SN in either the Parkinson disease or control group.

Discussion

The SN is a pair of tilted platelike structures that lie within the midbrain. It is located between the crural fibers and the red nucleus. The SN runs in the anterosuperolateral aspect to the posteroinferomedial aspect through the entire midbrain, and it is located mainly beneath the red nucleus (11). The SN is divided into two parts: a dorsal cell-dense part, the SNc, and a ventral cell-sparse part, the SNr. Neurons pigmented by neuromelanin in the SNc contain high concentrations of dopamine and are known as a principal source of striatal dopamine. On the other hand, neurons in SNr involve γ-aminobutyric acid (GABA) (ie, they are GABA-ergic), and they project to the thalamus and the pedunculopontine tegmental nucleus (11).

Drayer et al (1) originally introduced the MR anatomy of the SN on axial T2-weighted SE images through the upper midbrain. The hypointense areas represent the SNr and the red nucleus because of their high iron concentration. A band of relative hyperintensity between the hypointense SNr and red nucleus represents the SNc, which contains half the iron of the SNr (1, 15). This finding has been supported by that of other investigators who used gradient-echo, fast SE, and diffusion-weighted echo-planar imaging techniques (3, 4, 16–20). The hypointense area, considered to be the SNr, is not evident at the level of lower midbrain in which the SNr does exist in anatomic specimens; to our knowledge, this discrepancy has not been described.

In MR textbooks, the SN is described as structures of hyperintense gray matter that are anteroinferolateral to the red nucleus on proton density–weighted or STIR images (5–7). Its configuration and location agree well with those in the corresponding anatomic specimens (5–12). On axial images, hyperintense gray matter suggestive of the SN is evident at the level of the lower as well as in the upper midbrain. MR microscopic findings in fixed brain specimens are the same (8, 9). In this study, the SN was depicted as a tilted bandlike structure with hyperintense gray matter on proton density–weighted and fast STIR images, as previously reported. The location of this structure was exactly the same as that seen in brain specimens and anatomic textbooks. Moreover, the corresponding structure was not visible on T2-weighted images.

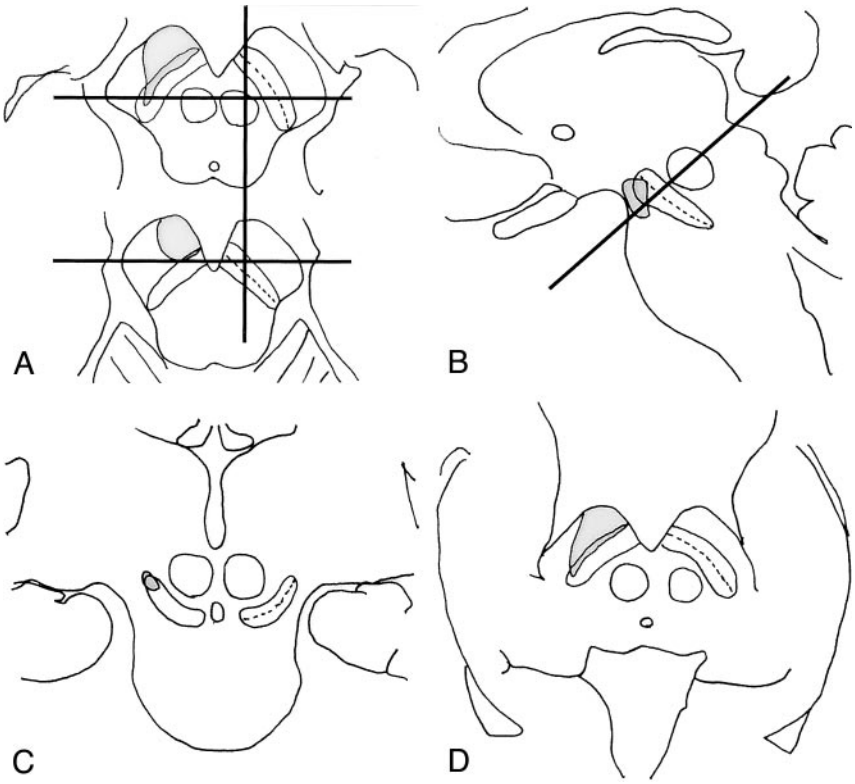

FIG 7. Schematic drawings of the multiplanar localization of the area of hyperintense gray matter on proton density–weighted and fast STIR images and of the hypointense area on the T2-weighted images (shaded area). The hypointense area on the T2-weighted image includes the crural fibers and only the anterosuperior potion of the SN. The *dotted line* indicates the presumable boundary between the SNr and the SNc.

A, Axial plane through the upper and lower midbrain.

B, Sagittal plane.

C, Coronal plane.

D, Oblique coronal plane.

TABLE 1: Signal Intensity of the SN and Related Structures

Structure	Signal Intensity*	
	On T2-Weighted Images	On Proton /Density–/Weighted and Fast STIR Images
Crus cerebri	WM/LSI†	WM
SNr	WM/LSI‡	GM
SNc	WM	GM
Prerubral white matter	WM	WM
Red nucleus	LSI	WM

* GM indicates gray matter signal intensity; LSI, low signal intensity; WM, white matter signal intensity.

† Only the medial part.

‡ Only the anterosuperior part.

Recently, abnormal signal intensity in the SN has been reported in cases of St Louis encephalitis and nigral degeneration secondary to striatal infarction (21, 22). In these cases, lesions with abnormal signal intensity were observed mainly beneath the red nucleus; the location and configuration were the same as our findings. These previous reports also support our results. Proton density–weighted and STIR images, and not T2-weighted images, seem to enable the direct visualization of the SN as a gray matter structure, although they cannot be used to distinguish the SNr from the SNc.

To our knowledge, this is the first report that correlates findings of the SN on T2-weighted images with findings on proton density–weighted and STIR images. In the present study, the hypointense area on T2-weighted images, which had been believed to be the SNr, did not correspond to the anterior half of the gray matter structure that presumably represented the SN on proton density–weighted and STIR images. It was mainly located in the medial part of the crural fibers and the anterosuperior margin of the hyperintense gray matter area. Therefore, we believe that the hypointense area on T2-weighted images is not identical to the SNr.

A short T2 relaxation time in the deep nuclei is reported to be largely dependent on the iron concentration (1). However, some investigators have shown that T2 values in brain structures are poorly associated with iron concentration. The signal intensity of iron-containing structures depends not only on the amount of iron but also on its physical state, its microscopic distribution, and its diffusion in the surrounding tissue (23, 24). We revealed that the hypointense area in the upper midbrain does not correspond to the distribution of the SNr, but it includes medial parts of the crural fibers, although the iron concentration in the SNr is higher than that in the crus cerebri (25). We do not have good explanation for why the crural fibers partly show strong signal-intensity attenuation.

Changes in the SN in Parkinson disease and secondary parkinsonism have been reported previously (2–4, 14, 16–20, 26–29). Several investigators have noted signal-intensity attenuation in the hypointense area on T2-weighted images (17, 18, 26). Others describe a reduction in the width of the hyperintense band on T2-weighted images and suggest that it may represent volume loss in the SNc or increased iron accumulation in the SNr (2–4, 14, 17, 19, 26, 27). Restoration of the low signal intensity on T2-weighted images is also reported (2) and is explained

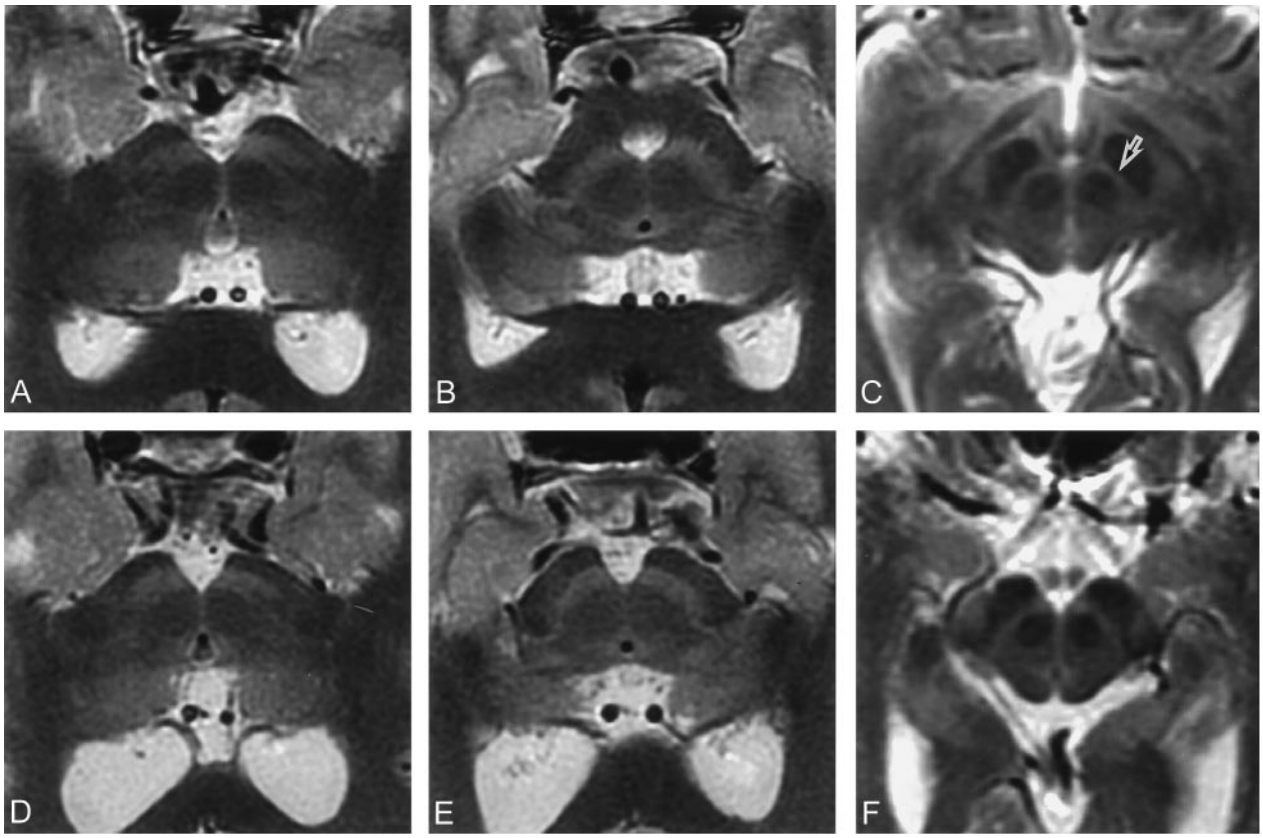

FIG 8. On fast STIR images, volume loss in the SN was not evident in patients with Parkinson disease. On T2-weighted images, thinning of the relatively hyperintense structure (*arrow* in *C*) was not evident in patients with Parkinson disease.

A–C, Images in a patient with Parkinson disease, a 52-year-old woman. Oblique coronal fast STIR images through the level of the posterior commissure (*A*) and superior colliculus (*B*) and axial T2-weighted image (*C*).

D–F, Corresponding images in a control subject, a 55-year-old woman.

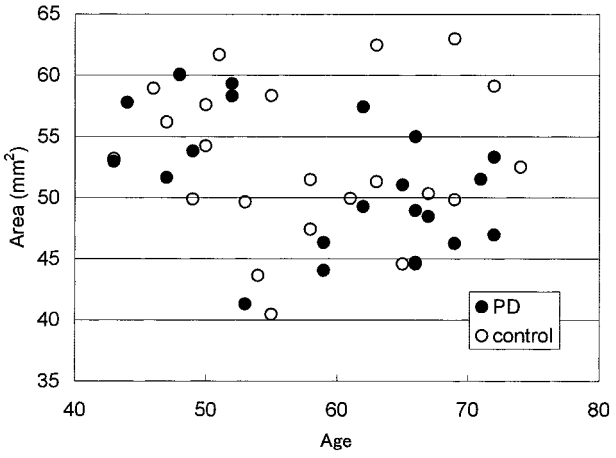

FIG 9. Area of the SN in Parkinson disease .

by iron depletion due to increased metabolic activity or by neuronal death with expansion of the extracellular space. However, many reports contradict the aforementioned results. Large overlaps or no significant difference is observed in the hyperintense band width or signal-intensity restoration in patients with Parkinson disease compared with control subjects (14, 19, 20, 26, 27). Moreover, all of these studies involved the use of axial images that were not perpendicular to the SN; with these, partial-volume effects cannot be avoided. In addition, only T2-weighted or T2*-weighted images were evaluated.

TABLE 2: Changes of the SN in patients with Parkinson disease

Change	Parkinson Disease Group (n = 22)	Control Group (n = 22)
Area of the SN, mm^2	51.2 ± 5.1*	53.1 ± 6.2
Area of the midbrain, mm^2	553 ± 40*	587 ± 58
SN/midbrain, %	9.3 ± 0.1*	9.1 ± 0.1
Thickness of SN, mm	4.3 ± 0.4*	4.4 ± 0.4
Width of hyperintense band on T2 Weighted images, mm	1.6 ± 0.2*	1.7 ± 0.3

* $P > .05$, compared with value in control subjects.

Despite recent advances in MR technology, the SN has never been evaluated directly. To our knowledge, this is the first report to measure the visible SN with in vivo MR imaging. Instead of T2-weighted SE images, we used proton density–weighted and fast STIR images to eliminate iron-related magnetic susceptibility effects and to enhance gray matter–white matter contrast. We did not use axial images but instead used oblique coronal images perpendicular to SN to avoid partial-volume effects, which are notable on axial images. However, we did not find any significant differences in the size of the SN between patients with Parkinson disease and control subjects. Parkinson dis-

ease is pathologically characterized by the loss of pigmented neurons and by the presence of Lewy bodies in the SN (30–33). However, recent pathologic studies reveal that the size of the SNc is not significantly decreased in patients with Parkinson disease, despite remarkable neuronal cell loss (30, 31). Our results support these reports.

We used fast STIR images to investigate the SN because of its excellent gray matter–white matter and brain-CSF contrast. On STIR images, spin attenuation, and T1 and T2 relaxations synergistically affect image contrast, improving the gray matter–white matter and brain-CSF contrast (34). Although proton density–weighted images have excellent gray matter–white matter contrast, their brain-CSF contrast is much lower than that of STIR images, and this is a disadvantage of proton density–weighted imaging in measuring the area of the SN. Compared with conventional STIR sequences, fast STIR sequences have an improved overall image quality and a shorter imaging time (35, 36). Blurring artifacts are observed with fast imaging because of T2 decay during k-space sampling. However, blurring can be minimized with short echo intervals, tailored radio frequencies, and k-space scrolling (37).

One of the limitations of this study was the relatively mild Parkinson disease in the patient group compared with the disease in previous reports (2–4). Some have reported that the clinical severity of Parkinson disease is strongly correlated with the width of the hyperintense band on T2-weighted images (27). The lack of thinning of the hyperintense band on T2-weighted images in this study may have been due to the mildness of the disease in the Parkinson disease group. Another limitation of this study is the relatively low spatial resolution. We used conventional SE images because the iron-related signal-intensity attenuation was better detected on conventional SE images than on fast SE images. To improve the spatial resolution by reducing the FOV or section thickness in the conventional SE technique is different because of its long acquisition time. A positive correlation exists between the field strength and signal-to-noise ratio or iron-dependent transverse relaxation rate (23). By using a high-field-strength machine, high-resolution SE images can be obtained with an excellent signal-to-noise ratio and with strong iron-related signal-intensity attenuation. We are now examining the SN by using a system equipped with a 3-T magnet. Another limitation of this study is that the SNr and SNc cannot be discriminated on proton density–weighted or fast STIR images, although the entire SN was visualized as a structure with gray matter signal intensity. Further investigation is needed to determine the substructures of the SN on MR images.

Conclusion

The SN is located beneath the red nucleus, and it can be directly identified as a hyperintense gray matter structure on proton density–weighted and fast STIR images. Axial T2-weighted images are not suitable for identifying the SN. We did not find significant differences in the size of the SN between patients with Parkinson disease and volunteers in the healthy control group in the quantitative evaluation of oblique coronal fast STIR images perpendicular to SN.

Acknowledgment

The authors gratefully thank Takashi Abe, MD, for his support in the clinical evaluation of the patients.

References

1. Drayer B, Burger P, Darwin R, Riederer S, Herfkens R, Johnson GA. **Magnetic resonance imaging of brain iron.** *AJNR Am J Neuroradiol* 1986;7:373–380
2. Rutledge JN, Hilal SK, Silver AJ, Defendini R, Fahn S. **Study of movement disorders and brain iron by MR.** *AJNR Am J Neuroradiol* 1987;8:397–411
3. Duguid JR, Paz RDA, DeGroot J. **Magnetic resonance imaging of the midbrain in Parkinson's disease.** *Ann Neurol* 1986;20:744–747
4. Braffman BH, Grossman RI, Goldberg HI, et al. **MR imaging of Parkinson disease with spin-echo and gradient-echo sequences.** *AJNR Am J Neuroradiol* 1988;9:1093–1099
5. Schnitzlein HN, Murtagh FR. *Imaging Anatomy of the Head and Spine.* Baltimore: Urban & Schwarzenberg; 1985:7–184
6. Mills CM, Groot JD, Posin JP. *Magnetic Resonance Imaging: Atlas of the Head, Neck, and Spine.* Philadelphia: Lea & Febiger; 1988: 3–108
7. Daniels DL, Haughton VM, Naidich TP. *Cranial and Spinal Magnetic Resonance Imaging.* New York: Raven Press; 1987:35–196
8. Hirsch WL, Kemp SS, Martinez AJ, Curtin H, Latchaw RE, Wolf G. **Anatomy of the brainstem: correlation of in vitro MR images with histologic sections.** *AJNR Am J Neuroradiol* 1989;10:923–928
9. Solsberg MD, Fournier D, Potts DG. **MR imaging of the excised human brainstem: a correlative neuroanatomic study.** *AJNR Am J Neuroradiol* 1990;11:1003–1013
10. Hayman LA. *Clinical Brain Imaging: Normal Structure and Functional Anatomy.* St Louis: Mosby 1992;53–214
11. Carpenter MB, Sutin J. *Human Neuroanatomy.* 4th ed. Baltimore: Williams & Wilkins; 1991:192–223
12. Williams PL, Bannister LH, Berry MM, et al. *Gray's Anatomy.* 38th ed. New York: Churchill Livingstone; 1995:1066–1073
13. Talairach J, Tournoux P. *Co-Planar Stereotaxic Atlas of the Human Brain.* New York: Thieme Medical Publishers 1988:43–45
14. Doraiswamy PM, Shah SA, Husain MM, et al. **Magnetic resonance evaluation of the midbrain in Parkinson's disease.** *Arch Neurol.* 1991;48:360
15. Jellinger K, Paulus W, Grundke-Iqbal I, Riederer P, Youndim MBH. **Brain iron and ferritin in Parkinson's and Alzheimer's diseases.** *J Neural Transm* 1990;2:327–340
16. Drayer BP, Olanow W, Burger P, Johnson GA, Herfkens R, Riederer S. **Parkinson plus syndrome: diagnosis using high field MR imaging of brain iron.** *Radiology* 1986;159:493–498
17. Gorell JM, Ordidge RJ, Brown GG, Deniau JC, Budere NM, Helpern JA. **Increased iron-related MRI contrast in the substantia nigra in Parkinson's disease.** *Neurology* 1995;45:1138–1143
18. Antonini A, Leenders KL, Meier D, Oertel WH, Boesiger P, Anliker M. **T2 relaxation time in patients with Parkinson's disease.** *Neurology* 1993;43:697–700
19. Huber SJ, Chakeres DW, Paulson GW, Khanna R. **Magnetic resonance imaging in Parkinson's disease.** *Arch Neurol* 1990;47:735–737
20. Adachi M, Hosoya T, Haku T, Yamaguchi K, Kawanami T. **Evaluation of the substantia nigra in patients with Parkinsonian syndrome accomplished using multishot diffusion weighted MR imaging.** *AJNR Am J Neuroradiol* 1999;20:1500–1506
21. Felix C, Borna M, James PL, Dennis B, James LF. **St. Louis encephalitis and the substantia nigra: MR imaging evaluation.** *AJNR Am J Neuroradiol* 1999;20:1281–1283
22. Ogawa T, Okudera T, Inugami A, et al. **Degeneration of the ipsilateral substantia nigra after striatal infarction: evaluation with MR imaging.** *Radiology* 1997;204:847–851
23. Gelman N, Gorell JM, Barker PB, et al. **MR imaging of human brain at 3.0T: preliminary report on transverse relaxation rates and relation to estimated iron content.** *Neuroradiology* 1999;210: 759–767

24. Chen JC, Hardy PA, Clauberg M, et al. **T2 values in the human brain: comparison with quantitative assays of iron and ferritin.** *Radiology* 1989;173:521–526
25. Temlett JA, Landsberg JP, Watt F, Grime GW. **Increased iron in the substantia nigra compacta of the MPTP-lesioned hemiparkinsonian African green monkey: evidence from proton microprobe elemental microanalysis.** *J Neurochem* 1994;62:134–146
26. Stern MB, Braffman BH, Skolnick BE, Hrutig HI, Grossman RI. **Magnetic resonance imaging in Parkinson's disease and parkinsonian syndrome.** *Neurology* 1989;39:1524–1526
27. Pujol J, Junque C, Vendrell P, Grau JM, Capudevila A. **Reduction of the substantia nigra width and motor decline in aging and Parkinson's disease.** *Arch Neurol.* 1992;49:1119–1122
28. Vymazal J, Righini A, Brooks RA, et al. **T1 and T2 in the brain of healthy subjects, patients with Parkinson disease, and patients with multiple system atrophy: relation to iron content.** *Radiology* 1999;211:489–495
29. Yagishita A, Oda M. **Progressive supranuclear palsy: MRI and pathological findings.** *Neuroradiology* 1996;38:S60–S66
30. Ma SY, Roytta M, Rinne JO, Collan Y, Rinne UK. **Correlation between neuromorphometry in the substantia nigra and clinical features in Parkinson's disease using disector counts.** *J Neurol Sci* 1997;151:83–87
31. German DC, Manaye K, Smith WK, Woodward DJ, Saper CB. **Midbrain dopaminergic cell loss in Parkinson's disease: computer visualization.** *Ann Neurol* 1989;26:507–514
32. Ma SY, Rinne JO, Collan Y, Roytta M, Rinne U. **A quantitative morphometrical study of neuron degeneration in the substantia nigra in Parkinson's disease.** *J Neurol Sci* 1996;140:40–45
33. Oppenheimer DR. **Diseases of the basal ganglia, cerebellum and motor neurons.** In: Adams HJ, Corsellis JAN, Duchen LW, eds. *Greenfield's Neuropathology*. 4th ed. New York: Wiley; 1984:699–747
34. Andrew JD, Joceph AF, Victor JS, James WR, Ann MH, John LD. **Short-TI inversion-recovery pulse sequence: analysis and initial experience in cancer imaging.** *Radiology* 1988;168:827–836
35. Constable RT, Reinhold C, McCauley T, Lange RC, Smith RC, McCarthy S. **Fast spin echo STIR imaging.** *J Comput Assist Tomogr* 1994;18:209–213
36. Hittmair K, Mallek R, Prayer D, Schindler EG, Kollegger H. **Spinal cord lesions in patients with multiple sclerosis: comparison of MR pulse sequences.** *AJNR Am J Neuroradiol* 1996;17:1555–1565
37. Sze G, Kawamura Y, Negishi C, et al. **Fast spin-echo MR imaging of the cervical spine: influence of echo train length and echo spacing on image contrast and quality.** *AJNR Am J Neuroradiol* 193;14:1203–1213